Research Paper

Promoted effect of alkalization on the catalytic performance of Rh/alk-Ti$_3$C$_2$X$_2$ (X=O, F) for the hydrodechlorination of chlorophenols in base-free aqueous medium

Mei Ming [a,1], Yanlin Ren [c,1], Min Hu [a], Yun Zhang [a,*], Ting Sun [a], Yuling Ma [a], Xiaojing Li [c], Weidong Jiang [b], Daojiang Gao [a], Jian Bi [a], Guangyin Fan [a,*]

[a] College of Chemistry and Materials Science, Sichuan Normal University, Chengdu, 610068, China
[b] School of Chemistry and Environmental Engineering, Sichuan University of Science & Engineering, Zigong 643000, China
[c] College of Chemistry and Chemical Engineering, China West Normal University, Nanchong 637009, China

ARTICLE INFO

ABSTRACT

Exploring MXenes as supports for synthesis of highly efficient catalysts are extremely important for hydrodechlorination of chlorophenols because of the acute toxicity and strong potential bioaccumulation of chlorophenols. We reported a facile strategy to synthesize Rh nanoparticles deposited on 2D alk-Ti$_3$C$_2$X$_2$ (X = O, F) (alk-Ti$_3$C$_2$X$_2$ for short) MXene, which was prepared through the removal of the Al layers of Ti$_3$AlC$_2$ and post-treatment by alkalization. Modifying the Ti$_3$C$_2$X$_2$ support by alkalization triggered the substitution of surface fluorine groups with surface oxygen species. The changes in the surface chemistry of alk-Ti$_3$C$_2$X$_2$ effectively prevented particle aggregation to form well-dispersed Rh nanoparticles in small sizes with relative high metal dispersion, thereafter improving the hydrogen uptake capacity of the catalyst. Consequently, the Rh/alk-Ti$_3$C$_2$X$_2$ catalyst significantly enhanced the catalytic performance for the HDC reaction, which could be assigned to the large number of active components from small Rh nanoparticles. This strategy provides a basis for investigating the use of MXenes as supports to synthesize well-defined metal nanoparticles in 2D layered structures for potential applications.

© 2017 Elsevier B.V. All rights reserved.

1. Introduction

Chlorophenols (CPs) are harmful organic contaminants that exhibit acute toxicity and strong bioaccumulation potential [1]. The degradation of CPs has been an important and urgent subject considering the increasing concern for environmental protection. Methods commonly used in CP decomposition include thermal and/or chemical oxidation, which lead to release of other highly toxic halogenated chemicals, such as dioxins and phosgene [2]. Scholars have developed approaches to effectively eliminate these pollutants without generating poisonous by-products. Catalytic hydrodechlorination (HDC) via hydrogen-mediated C—Cl bond scission is an interesting route to degrade CP contaminants by using low catalyst dosage and mild operation conditions [3–8].

Aqueous HDC of CPs has been successfully accomplished using various heterogeneous catalysts, especially supported catalysts with noble metals such as Pd [4,7–17], Pt [10,15,18] and Rh [4,10,12,14,15,19]. Despite its high cost and limited availability, Rh has attracted increasing interest as a suitable component for HDC of CPs. Rh exhibits unique catalytic properties, such as high resistance to acid and base attack and stability under severe reaction conditions [19,20]. These characteristics of Rh are vital considering that HDC of CPs is conducted in acidic environments because of HCl formation via the scission of C—Cl bonds of CPs. The produced phenol can be further hydrogenated into high-valued cyclohexanone (C-one) and cyclohexanol (C-nol) over Rh-based catalysts under mild conditions [21]. Supports significantly affect the catalytic property of heterogeneous catalysts by improving the chemical and environmental stabilities and/or the recyclability of active sites. Previous studies used carbon [15,22–24], Al$_2$O$_3$ [14,18,24,25], magnetic materials [26], and pillared clays [10,27] as carriers for preparing a series of catalysts for HDC of CPs. However, the catalytic activities of these catalysts were not satisfied enough and/or required large amounts of bases. Moreover, 2D graphene-supported metal NPs were excellent catalysts for the HDC of CPs under base-free conditions [21,28]. However, preparation of graphene was tedious, complicated and expensive, thereby limiting its practical applications.

Recently, a group of 2D graphene-like transition metal carbides and carbonitrides, known as MXenes, have drawn fast-growing interests because of their excellent structural and chemical properties such as hydrophilicity of the surface, chemical stability, and environment friendliness [29–34]. Importantly, convenient and large-scale preparation of MXene can be obtained by etching component A in MAX phases (of the general formula $M_{n+1}AX_n$, where M refers to an early transition metal, A represents group 13 or 14 elements, X represents C and/or N and n = 1, 2, or 3) [35]. Typically, Ti_3C_2 MXene is produced through removal of the Al layers of Ti_3AlC_2 by breaking the relatively weak Ti—Al bonds in hydrofluoric acid (HF). The formula $Ti_3C_2X_2(X=O, F)$ is used to express the introduction of OH or F groups to the exterior of Ti_3C_2 after Al-removal [34]. The abundant surface groups of $Ti_3C_2X_2$ benefit the attachment of metal NPs. To date, Au, Ag and Pd/MXene catalysts have been prepared and applied in lithium-ion batteries and surface-enhanced Raman spectroscopy (SERS) [36,37]. However, the particle sizes of metal NPs are not well controlled and relatively large. As such, MXene supported metal NPs with small sizes must be prepared to achieve superior catalytic activity for potential catalytic applications.

MXene-supported metal NPs may possess superior performance in the HDC reaction considering their characteristics of hydrophilic surface, chemical stability, and environment friendliness. Bearing this in mind, we reported a facile method to prepare Rh NPs anchored on alk-$Ti_3C_2X_2$ matrix, which was produced through etching the Al atoms of Ti_3AlC_2 in HF solution, and followed by post-treatment in alkali solution. The promoted effects of alkalization on the catalytic activity and stability of Rh/alk-$Ti_3C_2X_2$ in the HDC of 4-CP were investigated. It was discovered that alkalization was important to increase the number of oxygen-containing groups on the surface of $Ti_3C_2X_2$. During reduction, the interaction of oxygen-containing groups with Rh precursors formed small Rh NPs with good dispersion and abundant electron-deficient Rh species on the alk-$Ti_3C_2X_2$ matrix. The Rh/alk-$Ti_3C_2X_2$ catalyst with numerous small Rh NPs provided large surface active sites for efficient HDC of CPs. As a result, the Rh/alk-$Ti_3C_2X_2$ catalyst showed high catalytic activity toward the HDC of 4-CP at 30 °C and hydrogen balloon pressure in the base-free medium. Furthermore, the post-treatment of $Ti_3C_2X_2$ conferred the Rh/alk-$Ti_3C_2X_2$ with high activity and good recyclability under mild conditions in base-free aqueous media. This facile strategy to synthesize well-dispersed Rh NPs in the alk-$Ti_3C_2X_2$ matrix provides a basis for manufacture of a wide range of novel catalysts for HDC reaction.

2. Experimental

2.1. Chemicals

$RhCl_3 \cdot nH_2O$ was obtained from Kunming Institute of Precious Metals, China. Sodium borohydride ($NaBH_4$), sodium hydroxide (NaOH), and concentrated HF (40 wt%) were also purchased from Aladdin Industrial Inc., China. Other solvents were purchased from Aladdin Industrial Inc., China. Hydrogen gas with purity of 99.999% was supplied by Chengdu Taiyu Gas Co. Ltd., China. All reagents were used directly as received and without further purification. Ultrapure deionized water (18.2 MΩ) was used in all experiments.

2.2. Synthesis of $Ti_3C_2X_2$

MXene $Ti_3C_2X_2$ was prepared using a one-step approach by immersing the raw material Ti_3AlC_2 into HF solution at room temperature. Manipulation was conducted in a fume hood because of emission of poisonous gases. Containers made of polytetrafluoroethylene (PTFE) were used due to the high corrosiveness of HF aqueous solution. Typically, 5 g of Ti_3AlC_2 was slowly added to a

250 mL plastic beaker containing 80 mL of HF solution. The suspension was stirred at room temperature for 24 h. A black solid was collected by centrifugation and washed with 30 mL of water and 30 mL of absolute ethanol for three times. The solid was then dried in a vacuum oven at 60 °C for 12 h. The product, designated as $Ti_3C_2X_2$ (X = O, F), was stored in a 20 mL vial under argon atmosphere for characterization and catalyst preparation.

2.3. Post-treatment of $Ti_3C_2X_2$

$Ti_3C_2X_2$ was post-treated by alkalization before it was used as support to deposit Rh NPs. Typically, 1.0 g of $Ti_3C_2X_2$ was immersed into 50 mL of 1 M NaOH aqueous solution at 60 °C for 4 h. The solid $Ti_3C_2X_2$ was separated from the suspension by centrifugation and washed with distilled water and ethanol several times. The solid was then dried in a vacuum oven at 60 °C for 12 h. The product was labeled as alk-$Ti_3C_2X_2$.

2.4. Synthesis of catalysts

Rh NPs deposited on alk-$Ti_3C_2X_2$ were synthesized by impregnation with $NaBH_4$ as reducing agent. Briefly, 0.15 g of alk-$Ti_3C_2X_2$ was dispersed into 15 mL of distilled water and ultrasonicated for 2 h to achieve a uniform suspension. The $RhCl_3$ aqueous solution was slowly added under vigorous stirring, followed by drop-wise addition of the $NaBH_4$ aqueous solution. After completing the reduction, the obtained inky slurry was stirred overnight. The black solid was collected by repeated centrifugation and washed with water and ethanol several times. The back solid was dried in a vacuum oven at 60 °C for 12 h to form Rh/alk-$Ti_3C_2X_2$. The Rh loadings of Rh/alk-$Ti_3C_2X_2$ and Rh/$Ti_3C_2X_2$ estimated by ICP were approximately 4.42 and 4.46 wt%, respectively. For comparison, Rh/Ti_3AlC_2 catalyst with Rh loading of 4.75 wt% was prepared using the similar method.

2.5. Activity test

The catalytic activities of Rh/$Ti_3C_2X_2$ and Rh/alk-$Ti_3C_2X_2$ were investigated for the HDC of 4-CP at 30 °C and hydrogen balloon pressure. In a typical reaction, 5.0 mg of Rh/alk-$Ti_3C_2X_2$ and 5.0 mL of aqueous solution of 4-CP (Concentration: 1.5 g/L) were transferred into a 25 mL two-necked round-bottom flask equipped with a hydrogen balloon. The flask was vacuumed and flushed with pure hydrogen several times. The reaction temperature was maintained at 30 °C by using a water bath. The HDC of 4-CP was conducted at an agitation speed of 1200 rpm. During the reaction, samples were withdrawn using a syringe at an interval of 10 min. The conversion efficiency of 4-CP was analyzed by GC (Agilent 7890A). Other CPs, including monochlorophenol (2-CP and 3-CP), dichlorophenol (2,4-DCP, 2,6-DCP), and trichlorophenol (2,4,6-TCP), were used at a concentration of 1.5 g/L to study the general applicability of the Rh/alk-$Ti_3C_2X_2$ catalyst.

The reusability of the Rh/alk-$Ti_3C_2X_2$ catalyst was assessed in cycle test for the HDC of 4-CP under the optimized conditions comprising 30 °C and l atm H_2. After each run, the solid catalyst was recovered from the reaction mixture by centrifugation and washed with ethanol and water for three times. Fresh 4-CP aqueous solution was used for the next cycle.

2.6. Characterization of catalyst

The BET surface areas and pore volumes of the samples was analyzed by a Tristar 3020 Micromeritics instrument. H_2 chemisorption measurements were carried out using a Micromeritics AutoChem 2910 apparatus. Transmission electron microscopy (TEM) measurements were conducted using a FEI Tecnai G20 instrument at an accelerating voltage of 200 kV. X-ray diffraction

(XRD) patterns were recorded on a Rigaku X-ray diffractometer D/max-2200/PC equipped with Cu Kα radiation (40 kV, 20 mA) within 5°–50°. X-ray photoelectron spectra (XPS, Kratos XSAM800) were obtained using Al Kα radiation (12 kV and 15 mA) as an excitation source (hν = 1486.6 eV) and Au [binding energy (BE) Au$_{4f}$ = 84.0 eV] and Ag (BE Ag$_{3d}$ = 386.3 eV) as references. All BE values were referenced to the C1 s peak of contaminant carbon at 284.8 eV. Inductively coupled plasma-atomic emission spectrometry (ICP-AES) analysis was carried out on SPECTRO ARCOS spectrometer to determine the compositions of Ti, Al, and Rh in the samples. The quantification of chloride ion was conducted by an ion chromatography (ICS-90, DIONEX). The Cl balance was always closed around 98% during the HDC reaction.

3. Results and discussion

Fig. 1 illustrates the synthesis of Rh/alk-Ti$_3$C$_2$X$_2$. Ti$_3$AlC$_2$ was immersed into HF aqueous solution at room temperature for 24 h to remove the Al layers and form 2D Ti$_3$C$_2$X$_2$. The resulting Ti$_3$C$_2$X$_2$ was treated by alkalization in NaOH aqueous solution before being used as support for Rh NPs deposition. Consequently, the Rh^{3+} ions were captured on the surface of alk-Ti$_3$C$_2$X$_2$ through coordination with oxygen containing groups, such as hydroxyl and carboxyl [38]. Rh NPs were formed and anchored on the alk-Ti$_3$C$_2$X$_2$ surface by using NaBH$_4$ as reducing agent.

Table 1 illustrates the physicochemical properties of Ti$_3$AlC$_2$, Ti$_3$C$_2$X$_2$, alk-Ti$_3$C$_2$X$_2$, Rh/Ti$_3$C$_2$X$_2$ and Rh/alk-Ti$_3$C$_2$X$_2$. Ti$_3$AlC$_2$ possessed a low BET surface area of 3.9 m^2/g because of its closely aligned structure. The BET surface area of Ti$_3$C$_2$X$_2$ increased to 6.4 m^2/g after the removal of the Al layers in Ti$_3$AlC$_2$. The BET surface area of alk-Ti$_3$C$_2$X$_2$ was further increased to 8.6 m^2/g by alkalization. The BET surface areas of the two Rh-containing samples increased after the deposition of Rh. Specifically, Rh/alk-Ti$_3$C$_2$X$_2$ had larger BET surface area than Rh/Ti$_3$C$_2$X$_2$. The pore volumes of the investigated samples had the similar changing trend as the BET surface area. The increases of BET surface areas and pore volume of alk-Ti$_3$C$_2$X$_2$ were assigned to the intercalation of Ti$_3$C$_2$X$_2$ during the alkalization process. Similarly, the impregnation and reduction process could also cause intercalation of the supports, leading to the increase of the BET surface areas and pore volume. These results show that the Rh/alk-Ti$_3$C$_2$X$_2$ catalyst treated by alkalization process has large surface area. One can therefore assume that the obvious differences in the BET surface area of the catalysts may lead to a distinct catalytic performance.

SEM characterization was performed to determine the morphology of the pristine Ti$_3$AlC$_2$ and Ti$_3$C$_2$X$_2$ and identified the etching of Al layers in Ti$_3$AlC$_2$. As shown in Fig. 2a, Ti$_3$AlC$_2$ showed a closely aligned and layered structure. The successful exfoliation of Ti$_3$AlC$_2$ and the removal of Al layers were confirmed by observing the detriment of the closely aligned and layered structure in the HF solution (Fig. 2b). The resulting material exhibited a morphology similar to that of graphene, which was produced from exfoliation of graphite. The morphologies of Rh NPs deposited on Ti$_3$C$_2$X$_2$ and alk-Ti$_3$C$_2$X$_2$ were characterized through TEM analysis, and the results were illustrated in Figs. 2c and 2d. Rh NPs aggregated on the surface of Ti$_3$C$_2$X$_2$ without post-treatment. Interestingly, the aggregation of Rh NPs was inhibited when Ti$_3$C$_2$X$_2$ was treated with NaOH aqueous solution. Rh NPs, with size of 2–4 nm, were uniformly distributed on the surface of alk-Ti$_3$C$_2$X$_2$. Continuous lattice fringes were detected in the HRTEM image, indicating the successful attachment of Rh onto the alk-Ti$_3$C$_2$X$_2$ support. These data show that the morphology and particle sizes differ from Rh NPs synthesized with post-treatment of Ti$_3$C$_2$X$_2$ by alkalization and those without alkalization treatment. Moreover, the catalytic HDC reaction is sensitive to catalyst size [19]. The two catalysts prepared in this work are predicted to perform differently toward the

HDC reaction because of varied size of Rh NPs on the support. The Rh/alk-Ti$_3$C$_2$X$_2$ catalyst with high dispersion and small size Rh NPs are critical for improving catalytic performance.

XRD characterization was performed to check the phase structures of Ti$_3$AlC$_2$, Ti$_3$C$_2$X$_2$, alk-Ti$_3$C$_2$X$_2$, Rh/Ti$_3$C$_2$X$_2$, and Rh/alk-Ti$_3$C$_2$X$_2$. Fig. 3a shows the XRD patterns of the samples. The characteristic peaks of the pristine Ti$_3$AlC$_2$ matched with the standard XRD pattern of Ti$_3$AlC$_2$ (JCPDS no. 52-0875), confirming the high purity of the pristine Ti$_3$AlC$_2$. The XRD patterns also revealed the etching degree of the pristine Ti$_3$AlC$_2$. When Ti$_3$AlC$_2$ was soaked in HF aqueous solution at 25 °C for 24 h, the (104) characteristic peak (2θ = 39°) disappeared, indicating the removal of Al layers and the formation of 2D Ti$_3$C$_2$ layers. Concomitantly, the Al layers were replaced with oxygen-containing and/or fluoride functional groups, as confirmed by the shift of the (002) diffraction peak to 2θ = 9.0° because of structural expansion. The (002) peak of Ti$_3$C$_2$X$_2$ shifted to a low angle when the synthesized Ti$_3$C$_2$X$_2$ was treated in the alkali aqueous solution. This finding could be due to the intercalation of Na$^+$ ions when the Ti$_3$C$_2$X$_2$ sheets were treated in the alkali solution [29]. Compared with the pristine Ti$_3$C$_2$X$_2$, the attachment of Rh NPs led to the shift of the (002) peak in Rh/Ti$_3$C$_2$X$_2$, indicating the intercalation of the Rh ions during catalyst preparation. Furthermore, no noticeable shift of the (002) peak was observed when Rh NPs were deposited on alk-Ti$_3$C$_2$X$_2$, revealing that the attachment of Rh NPs did not change the structure of alk-Ti$_3$C$_2$X$_2$. These results suggest that the Rh ions preferentially intercalated in the interlayer galleries of Ti$_3$C$_2$X$_2$ during the preparation of Rh/Ti$_3$C$_2$X$_2$, whereas the Rh^{3+} ions were likely adsorbed on the surface of alk-Ti$_3$C$_2$X$_2$ because of Na$^+$ ion intercalation. The reduced Rh NPs were mainly located on the surface of 2D layers or the edge sites of alk-Ti$_3$C$_2$X$_2$ instead of the interlayer spaces. This difference may lead to a different catalytic property toward HDC reaction. Furthermore, the diffraction peaks associated with metallic Rh or other Rh species were not observed within the XRD detection limit in the two samples, indicative of the relatively low loading of Rh and/or high dispersion of Rh NPs on the carrier.

XPS survey scans of Rh/Ti$_3$C$_2$X$_2$ and Rh/alk-Ti$_3$C$_2$X$_2$ were recorded to investigate the changes in the surface chemistry of Rh/alk-Ti$_3$C$_2$X$_2$. In both samples, signals corresponding to O, F, C, Al, Ti, and Rh were observed. The surface atomic ratios are shown in Fig. 3b. The residual Al on the surface of all samples demonstrated that HF could not etch all Al species [34]. Al/Ti atomic ratios calculated from XPS analysis declined from 0.18 to 0.09 corresponding to the Al/Ti ratio decreased from 0.15 to 0.07 measured by ICP-AES. These findings revealed that the Al atoms in Ti$_3$C$_2$X$_2$ could be further removed in alkali aqueous solution for a period of time. Moreover, the decreasing F/Ti ratios from 0.39 to 0.20 accompanied by increasing O/Ti ratios after alkalization demonstrated that the F groups could be substituted by oxygen groups. The C1 s spectra of both samples were recorded to determine the oxygen-containing groups (Fig. 3c). The C1 s spectra of the samples could be fitted with four components, situated at 281.5, 284.8, 286.4, and 288.7 eV, which corresponded to the Ti—C, C—C, C—OH, and HO—C≡O groups, respectively (Fig. 3c) [39–42]. These results confirm that the oxygen-containing groups on the surface of Ti$_3$C$_2$X$_2$ and alk-Ti$_3$C$_2$X$_2$ are hydroxyl and carboxyl groups. The contents of the oxygen-containing groups including —OH and HO—C≡O in the Ti$_3$C$_2$X$_2$ and alk-Ti$_3$C$_2$X$_2$ supports were calculated to be 33.9 and 38.3% respectively. These results show that post-treatment of Ti$_3$C$_2$X$_2$ increased the number of oxygen-containing groups. The increase in the number of these groups after alkalization process may facilitate the attachment of Rh^{3+} on the surface of alk-Ti$_3$C$_2$X$_2$ via the coordination between Rh^{3+} and oxygen-containing groups. Furthermore, these groups can act as anchors to stabilize the generated Rh NPs during reduction. As a consequence, the surface atomic
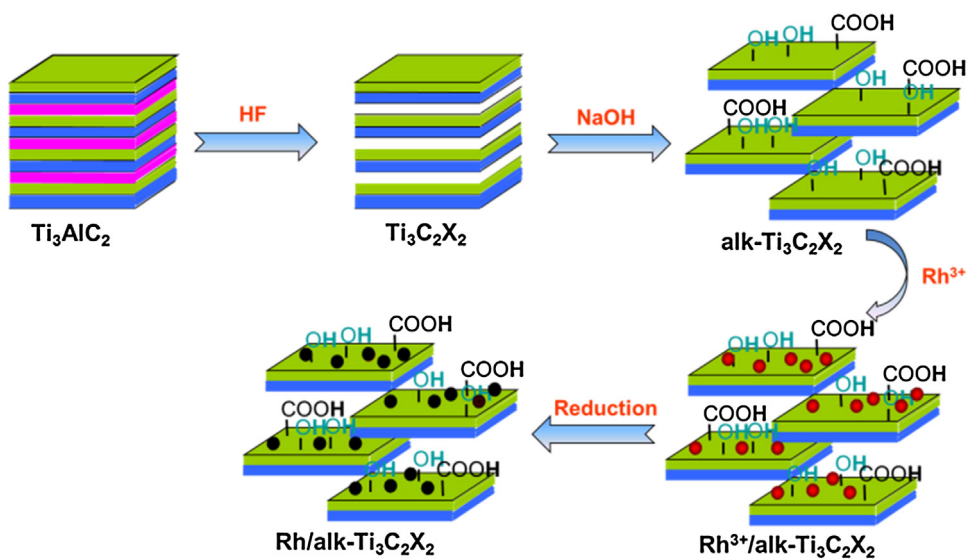
Fig. 1. The procedure for the synthesis of Rh/alk-Ti$_3$C$_2$X$_2$.

Table 1
Physicochemical and catalytic property of the investigated samples.

Samples	BET surface areas (m^2/g)	Pore volume $\times 10^2$ (cm^3/g)	H$_2$ chemisorption results		Rh^{n+}/Rh^{0}[a]	TOF (s^{-1})
			H$_2$ uptake (umol/g$_{cat}$)	%Rh[c] dispersion		
Ti$_3$AlC$_2$	3.9	1.0	n/a[b]	n/a	n/a	n/a
Ti$_3$C$_2$X$_2$	6.4	2.3	n/a	n/a	n/a	n/a
alk-Ti$_3$C$_2$X$_2$	8.6	3.1	n/a	n/a	n/a	n/a
Rh/Ti$_3$C$_2$X$_2$	13.0	5.9	37.0	17.1	0.50	0.09
Rh/alk-Ti$_3$C$_2$X$_2$	19.4	5.3	78.7	36.3	0.61	0.13

[a] Based on XPS results.

[b] n/a = not available.

[c] The metallic dispersion was calculated based on the assumption that one hydrogen atom adsorbed on one Rh site.

content of Rh is higher in the sample with the alk-Ti$_3$C$_2$X$_2$ support than that in Rh/Ti$_3$C$_2$X$_2$.

The chemical valence of the active sites of the catalyst is important for catalytic property. Therefore, the valence states of Rh in both samples were determined by high resolution XPS measurement. As illustrated in Fig. 3d, the Rh 3d core level spectra comprised those of Rh 3d$_{5/2}$ and Rh 3d$_{3/2}$ spin-orbit components; the peaks fitted well with six components. Regarding Rh 3d$_{5/2}$, the peaks at 307.0 ± 0.2 eV were ascribed to metallic Rh^0 3d$_{5/2}$ species. The other components located at 308.0 ± 0.2 eV and 309.8 ± 0.2 eV were assigned to electro-deficient Rh^{n+} species, including Rh (I) and Rh (III) species, in both samples [43,44]. The binding energies of Rh 3d$_{5/2}$ had almost the same values, indicating that the electronic structures of both Rh^{n+} and Rh^0 were less affected by the Ti$_3$C$_2$X$_2$ and alk-Ti$_3$C$_2$X$_2$ supports. Moreover, the atomic molar ratios of Rh^{n+}/Rh^0 (calculated from the integral peak area of fitted Rh^{n+} and Rh^0 components) in the Rh/alk-Ti$_3$C$_2$X$_2$ and Rh/Ti$_3$C$_2$X$_2$ samples were 0.61 and 0.50 respectively. The increasing Rh^{n+}/Rh^0 ratio in the Rh/alk-Ti$_3$C$_2$X$_2$ sample indicated that the Rh^{3+} ions were difficult to reduce when the support was treated in alkali solution because of the strong interaction between Rh ions and the high electronegativity of oxygen in the oxygen-containing groups in alk-Ti$_3$C$_2$X$_2$ [45]. XPS results show that the changes in the surface chemistry of alk-Ti$_3$C$_2$X$_2$ slightly increases the number of electro-deficient Rh species.

3.1. Catalytic HDC of CPs

The HDC of 4-CP produces phenol, C-one, and C-nol over Rh-based catalysts [19,21]. C-one and C-nol formed through a parallel-series pathway are favorable chemicals for industrial production [18,19]. Thus far, enhancing the catalytic HDC of 4-CP to obtain the desired products under base-free conditions remains challenging because of the deactivation of active components by HCl. The possible mass transfer limitations in present reaction system were firstly investigated before starting the catalyst activity tests. As well known, the mass transfer limitations consist of internal and external mass transfer limitations. In this work, the external particle mass transfer limitation could be discarded based on the results that the stirring velocity in the range from 1000 to 1400 rpm has no effect on 4-CP conversion [18]. Moreover, an estimation of the Weisz–Prater numbers (N_{W-P}) were carried out, and the values of N_{W-P} were always less than 0.3, indicating the negligible internal transfer limitations in the reaction system [46]. The catalytic properties of Rh/Ti$_3$C$_2$X$_2$ and Rh/alk-Ti$_3$C$_2$X$_2$ were studied for the HDC of 4-CP under base-free conditions at 30 °C and balloon hydrogen pressure with desired 4-CP (1.5 g/L) and catalyst concentrations (1.0 g/L) (Table S1). Water was chosen as solvent because of its superior catalytic activity for the HDC reaction (Table S2). As shown in Table 2, the catalysts performed differently toward the HDC of 4-CP. The Rh/alk-Ti$_3$C$_2$X$_2$ exhibited a conversion value of 82.2% and relatively high selectivity of 53.7% to C-nol and C-one within 20 min of reaction time. By contrast, the Rh/Ti$_3$C$_2$X$_2$ catalyst showed a lower conversion of 54.4% and a lower selectivity of 47.4% to C-nol and C-one under the same conditions. 4-CP was completely converted within 40 min and showed 82.9% selectivity toward C-nol and C-one. It was completely transferred to C-nol and C-one within 50 min. Nevertheless, the Rh/Ti$_3$C$_2$X$_2$ catalyst only provided a conversion of 98.6% with 100 min, despite that the selectivity of C-nol and C-one reached 90.2%. For comparison,
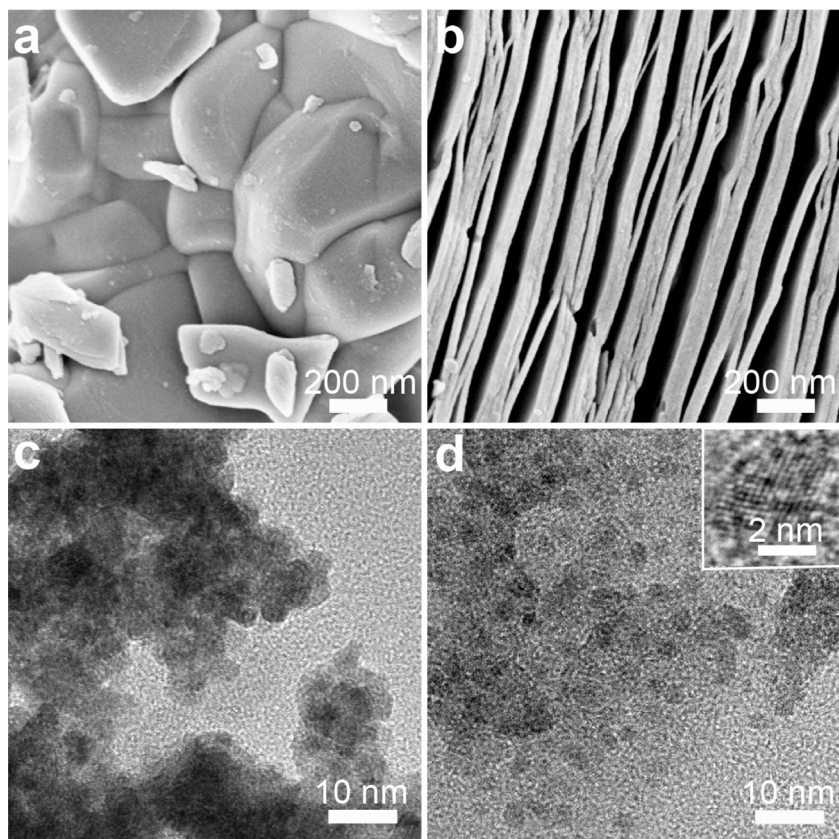
Fig. 2. SEM images of Ti_3AlC_2 and $Ti_3C_2X_2$ (a, b), and TEM images of $Rh/Ti_3C_2X_2$ (c) and $Rh/alk-Ti_3C_2X_2$ (d), inset is the HRTEM image.

Table 2
HDC of 4-CP with $Rh/Ti_3C_2X_2$ and $Rh/alk-Ti_3C_2X_2$ in base-free conditions.

Catalysts	Time (min)	Conversion (%)	Selectivity (%)		
			C-nol	C-one	phenol
$Rh/Ti_3C_2X_2$	20	54.4	8.1	39.3	52.6
	40	79.9	11.6	52.9	35.4
	60	91.6	13.6	61.1	25.3
	80	95.2	16.3	64	19.7
	100	98.6	17.3	73. 0	9.8
$Rh/alk-Ti_3C_2X_2$	10	54.5	3.7	33.5	62.8
	20	82.2	7.5	46.3	46.3
	30	90.8	8.5	56.1	35.5
	40	100	11.1	71.9	17.1
	50	100	13.5	86.5	0
	60	100	20.3	79.7	0

Reaction conditions: 1.5 g/L of 4-CP (5.0 mL), 1.0 g/L of catalyst, temperature, 30 °C, and hydrogen balloon pressure.

the Rh/Ti_3AlC_2 catalyst was also prepared and applied for the HDC of 4-CP at the same reaction conditions. The Rh/Ti_3AlC_2 catalyst exhibited a low conversion of 57.8% and selectivity of 40.7% to C-one and C-nol within 100 min (Table S3). The reaction rate constant k was utilized to evaluate the intrinsic kinetics of the HDC reaction. The k value for the HDC of 4-CP was calculated based on the pseudo-first-reaction kinetic model, where $\ln(C_t/C_0)$ changed linearly with reaction time (t) [47]. The rate constant of the Rh/Ti_3AlC_2 catalyst was 1.3×10^{-2} min^{-1}, whereas the $Rh/Ti_3C_2X_2$ catalyst had a higher k value of 4.1×10^{-2} min^{-1} (Fig. 4a). These results inferred the superiority of $Ti_3C_2X_2$, which were prepared by the exfoliation of Ti_3AlC_2 by using HF as etching agent. Furthermore, the Rh/alk-$Ti_3C_2X_2$ catalyst possessed the highest k value of 10.1×10^{-2} min^{-1} for the catalytic HDC of 4-CP (Fig. 4b), indicative of its high catalytic activity. Moreover, to evaluate the catalytic activity of the

catalysts, the turnover frequency (TOF) was calculated according to the method reported by Molina et al. [10]. The TOF values were calculated as Eq. (1), in which r^0 designated the initial rate (units: mmol/g_{metal}·min·), D was the metal dispersion (%) obtained from the H_2 chemisorption, and M_A denoted as the atomic mass of Rh (g/mol). The $Rh/Ti_3C_2X_2$ catalyst possessed an

$$TOF(s^{-1}) = \frac{r_0 \cdot M_A \times 10^{-3}}{D \cdot 60} \times 100 \qquad (1)$$

initial TOF value of 0.09 s^{-1}, while a higher TOF value of 0.13 s^{-1} was obtained with the Rh/alk-$Ti_3C_2X_2$ catalyst, indicating its high catalytic activity for the HDC of 4-CP. The initial reaction rate and TOF value of Rh/alk-$Ti_3C_2X_2$ determined in the present work was compared with that of the reported Rh-based catalysts for the HDC of CPs. Molina et al. [27] indicated an initial rate of 73.5 mmol/g_{Rh}·min under a continuous H_2 flow rate of 150 mL min^{-1}. The same authors
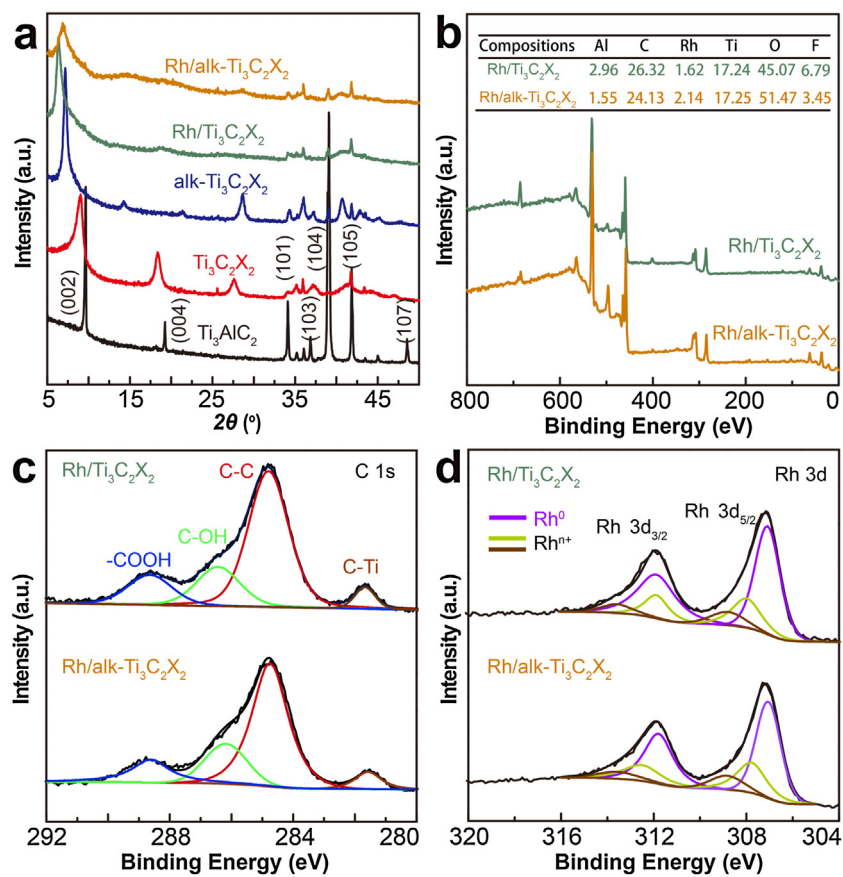
Fig. 3. XRD patterns of Ti_3AlC_2, $Ti_3C_2X_2$, alk-$Ti_3C_2X_2$, Rh/$Ti_3C_2X_2$, and Rh/alk-$Ti_3C_2X_2$ (a); XPS survey scans of Rh/$Ti_3C_2X_2$ and Rh/alk-$Ti_3C_2X_2$ (b) XPS spectra of C1 s peaks of Rh/$Ti_3C_2X_2$ and Rh/alk-$Ti_3C_2X_2$ (c), and Rh3d peaks of Rh/$Ti_3C_2X_2$ and Rh/alk-$Ti_3C_2X_2$ (d).
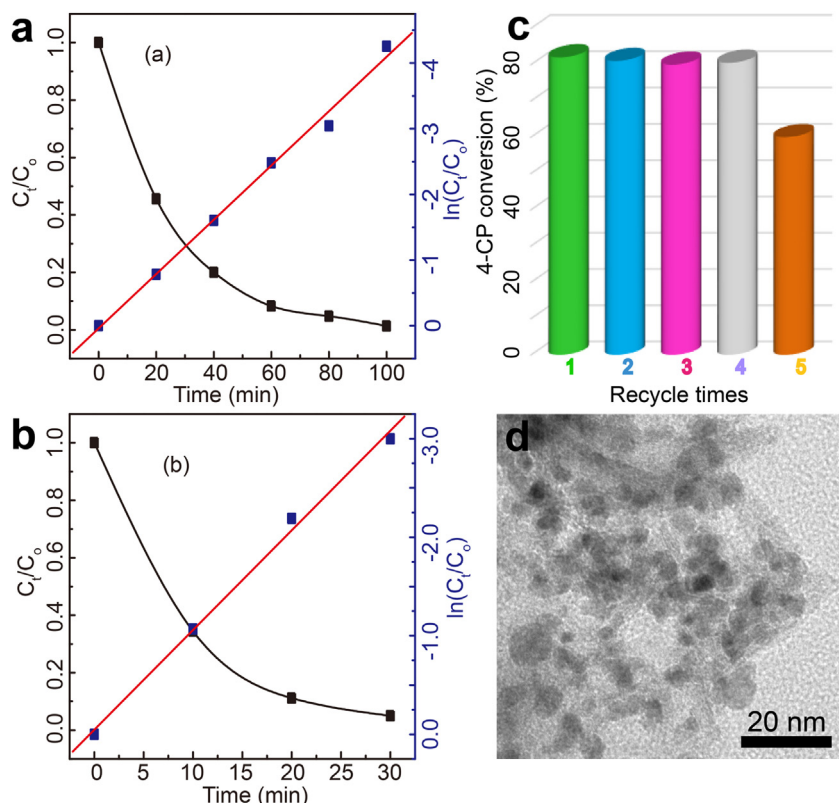
Fig. 4. Plots of C_t/C_0 and $\ln(C_t/C_0)$ versus time for 4-CP HDC over Rh/$Ti_3C_2X_2$(a) and Rh/alk-$Ti_3C_2X_2$(b); recyclability of Rh/alk-$Ti_3C_2X_2$(c) and TEM image of the Rh/alk-$Ti_3C_2X_2$ recycled for five times (d).

reported an optimal initial rate of 14.6 mmol/g_{Rh}·min and TOF value of 0.10 s^{-1} over pillared clays-supported Rh catalyst [10]. Diaz et al. [18] investigated the HDC of 4-CP by using Rh/Al$_2$O$_3$ catalyst with initial rates of 20.6 and 38.0 mmol/g_{Rh}·min at 20 °C and 40 °C, respectively. Yuan and Keane [48] obtained an initial reaction rate of 6.0 mmol/g_{Rh}·min in the HDC of 2,4-DCP at 0 °C by using Rh/C catalyst. Pozan and Boz [23] reported initial reaction rate of 0.018 mmol/g_{Rh}·min and a TOF value of 1.0 s^{-1} for the HDC of 2, 4-DCP at 85 °C over Rh/C catalyst. Baeza et al. [19] reported the HDC of 4-CP at 30–45 °C with activity values within 1.7–29.4 mmol/g_{Rh}·min with PVP-Rh catalysts. In the present work, we achieved an initial HDC rate of 26.5 mmol/g_{Rh}·min and a TOF of 0.13 s^{-1} for the HDC of 4-CP at 30 °C under base-free conditions by using a balloon hydrogen pressure.

To gain more insights on the reaction kinetics, the HDC of 4-CP were conducted under different temperatures with the other reaction conditions unchanged. The conversion of 4-CP gradually increased with the elevation of temperature from 293 to 308 K. The reaction constants at different temperature could be calculated by data fitting assumed that the HDC of 4-CP was a pseudo-first-order reaction. To this end, the reaction rate constant for the HDC of 4-CP over Rh/alk-Ti$_3$C$_2$X$_2$ at different temperatures could be explored to calculate the activation energy [49]. Fig.S1 shows the example of pseudo-first-order regression in the HDC of 4-CP by Rh/alk-Ti$_3$C$_2$X$_2$ with the temperature from 293 to 308 K. The rate constants were calculated on the basis of the slopes of the fitting straight lines (Fig.S1b). Consequently, the activation energy was estimated to be 56.6 kJ/mol for the HDC of 4-CP over Rh/alk-Ti$_3$C$_2$X$_2$. It has been reported that the chemical controlled reactions have relatively large activation (>29 kJ/mol) compared with the diffusion control ones [49]. The activation energy obtained in this study over Rh/alk-Ti$_3$C$_2$X$_2$ was greater than 29 kJ/mol, indicating that the HDC of 4-CP over Rh/Ti$_3$C$_2$X$_2$ is actually conducted under chemical control reaction [49], which is in good agreement with above results.

According to the experimental results, the alk-Ti$_3$C$_2$X$_2$ was a distinct and powerful carrier for synthesis of high-performance Rh-based catalysts. As discussed, the post-treatment of Ti$_3$C$_2$X$_2$ changed the surface chemistry of the alk-Ti$_3$C$_2$X$_2$ support including the surface area and the oxygen-containing functional groups. These changes were important in controlling the particle size of the Rh/alk-Ti$_3$C$_2$X$_2$ catalyst by prohibiting Rh NPs aggregation during their formation, as confirmed by the TEM results. The conclusion was also confirmed by the H$_2$ chemisorption, in which a relative high metallic dispersion was observed in Rh/alk-Ti$_3$C$_2$X$_2$ (36.3%) compared with the Rh/Ti$_3$C$_2$X$_2$ catalyst (17.1%). It has been reported that the HDC of CPs is a structure sensitive reaction [10,19,22,50,51]. The metallic dispersion, and consequently the metal particle size of the active phase were considered as one of the main factor affecting the catalytic HDC reactivity. For Rh-based supported catalysts, Diaz et al. found that the own-made catalyst with a particle size of 3.4 nm much higher catalytic activity and selectivity to C-nol than the commercial one with a particle size of 7.3 nm [22]. In another work, they also found that the supported Rh catalysts with metal particle size between 3.1 and 3.7 nm exhibited the highest catalytic activity, while the catalysts with the smallest particle size (<2.3 nm) showed poorer activity [52]. Moreover, it was discovered that the increase of particle size resulted in the decrease of catalyst reusability [21]. Generally, the variations of metal particle size could change the adsorption energies and give rise to quite different effects, from the catalyst poisoning to substrate activation, depending on the nature of surface adsorption between the molecule and metal particle[19]. On the other hand, the relative amounts of active sites of Rh on the two catalysts were calculated form H$_2$ chemisorption in Table 1. It can be seen that the Rh/alk-Ti$_3$C$_2$X$_2$ catalyst exhibited higher H$_2$ uptake than Rh/Ti$_3$C$_2$X$_2$. Accordingly, the Rh active sites were estimated

to be 9.5×10^{19} and 4.5×10^{19} sites/$g_{catalyst}$ for the Rh/alk-Ti$_3$C$_2$X$_2$ and Rh/Ti$_3$C$_2$X$_2$ catalysts, respectively. Consequently, the Rh/alk-Ti$_3$C$_2$X$_2$ catalyst with more Rh active sites facilitated the HDC of 4-CP. In addition, the difference in the amount of spillover hydrogen over different catalysts should be related to different catalytic performance. Therefore, the rate of the catalytic HDC of 4-CP catalyzed by Rh/alk-Ti$_3$C$_2$X$_2$ could be accelerated.

However, although the control experimental results presented in this work indicate that both of the Rh^0 and Rh^{n+} species are required for the HDC reaction (Tables S3 and S4), with the Rh catalysts the possible effect of the Rh^{n+}/Rh^0 ratio is much less pronounced compared with Pd based catalysts [52]. There is no a conclusive agreement on whether this reaction is sensitive to the Rh^{n+}/Rh^0 ratio of Rh catalysts. Considering the tiny difference in the Rh^{n+}/Rh^0 ratios between the two catalysts, the distinct differences in particle size, metal dispersion and hydrogen uptake are much more pronounced, which were responsible for the increase of catalytic activity of Rh/alk-Ti$_3$C$_2$X$_2$ in the HDC reaction. Further investigation should be conducted in the future to elucidate the influence of the Rh^{n+}/Rh^0 ratio on catalyst property of the Rh-based catalysts for the HDC reaction.

This technique was extended to HDC of other CPs to show the general applicability of Rh/alk-Ti$_3$C$_2$X$_2$. Table 3 illustrates the results of HDC of monochlorophenols, dichlorophenols, and trichlorophenols with Rh/alk-Ti$_3$C$_2$X$_2$. Complete HDC were observed in all cases, demonstrating the generality of Rh/alk-Ti$_3$C$_2$X$_2$ for CPs HDC reaction. The HDC of monochlorophenols could be achieved in a short reaction time, whereas the complete HDC of dichlorophenols and trichlorophenol required longer time. This phenomenon could be explained by the deactivation of the active sites of Rh/alk-Ti$_3$C$_2$X$_2$ due to the high HCl content formed during the HDC process.

The recycling ability of the catalyst is important for practical applications, apart from the high activity for the HDC reaction. We further explored the recyclability of Rh/alk-Ti$_3$C$_2$X$_2$ in the HDC of 4-CP in base-free aqueous medium. As illustrated in Fig. 4c, the HDC of 4-CP could be conducted with five successive runs under the same reaction conditions. Especially, the catalytic activity of Rh/alk-Ti$_3$C$_2$X$_2$ was maintained and no loss of catalytic activity was observed from the first to the fourth runs. However, the conversion of 4-CP decreased to about 60% in the fifth run, showing the decrease of catalytic activity. As detected by ICP-AES, the leaching of Rh was negligible (<1‰). The catalyst recycled for five times was collected and applied for TEM characterization. As can be seen from Fig. 4d, the particle size of Rh slight increased, which was responsible for the loss of catalytic activity. Even so, the catalyst has exhibited excellent tolerance toward the HDC of 4-CP reaction under the base-free conditions. These results demonstrate that the Rh/alk-Ti$_3$C$_2$X$_2$ catalyst exhibits excellent stability and reusability for the HDC of 4-CP, which makes it as a promising material for practical applications.

4. Conclusions

In conclusion, we reported the synthesis and catalytic activity of Rh/alk-Ti$_3$C$_2$X$_2$ for the HDC of CPs in base-free aqueous medium. The terminal fluorine on the surface of Ti$_3$C$_2$X$_2$ was substituted with oxygen-containing functional groups after alkalization. This change in surface chemistry of alk-Ti$_3$C$_2$X$_2$ played an important role in producing Rh NPs with small particle sizes and increased metal dispersion of Rh species on the surface of the support. The improved catalytic activity of Rh/alk-Ti$_3$C$_2$X$_2$ for the HDC of 4-CP by support alkalization could be attributed to the small particle size with relative high metal dispersion. Moreover, the apparent improvement of the catalytic property of Rh/alk-Ti$_3$C$_2$X$_2$ in 4-CP

Table 3
HDC of different substituted CPs by Rh/alk-Ti$_3$C$_2$X$_2$.

Substrates	Time (min)	Conversion (%)	Selectivity (%)		
			C-nol	C-one	phenol
4-CP	40	100.0	13.3	81.5	5.3
2-CP	50	100.0	14.6	78.7	6.7
3-CP	60	100.0	14.6	75.9	9.4
2,4-DCP	70	100.0	20.0	80.0	0
2,6-DCP	90	100.0	17.5	80.4	2.0
2,4,6-TCP	120	100.0	11.4	83.6	5.0

Reaction conditions: 1.5 g/L of CPs (5.0 mL), 1.0 g/L of catalyst, temperature, 30 °C, and hydrogen balloon pressure.

HDC demonstrated the successful application of alk-Ti$_3$C$_2$X$_2$ as catalyst support. These results are encouraging and will inspire the application of other MXenes in the field of catalysis.

Acknowledgements

Appendix A. Supplementary data

Supplementary data associated with this article can be found, in the online version, at http://dx.doi.org/10.1016/j.apcatb.2017.04.017.

References

[1] Z. Jin, C. Yu, X. Wang, Y. Wan, D. Li, G. Lu, Chem. Commun. (2009) 4438–4440.
[2] T. Hara, T. Kaneta, K. Mori, T. Mitsudome, T. Mizugaki, K. Ebitani, K. Kaneda, Green Chem. 9 (2007) 1246–1251.
[3] Q. Wang, J. Wang, D. Wang, M. Turhong, M. Zhang, Chem. Eng. J. 280 (2015) 158–164.
[4] A.H. Pizarro, V.M. Monsalvo, C.B. Molina, A.F. Mohedano, J.J. Rodriguez, Chem. Eng. J. 273 (2015) 363–370.
[5] Y. Liu, X. Li, X. Le, W. Zhang, H. Gu, R. Xue, J. Ma, New J. Chem. 39 (2015) 4519–4525.
[6] Y. Liu, Z. Dong, X. Li, X. Le, W. Zhang, J. Ma, RSC Adv. 5 (2015) 20716–20723.
[7] Z. Dong, X. Le, C. Dong, W. Zhang, X. Li, J. Ma, Appl. Catal. B 162 (2015) 372–380.
[8] Z. Dong, C. Dong, Y. Liu, X. Le, Z. Jin, J. Ma, Chem. Eng. J. 270 (2015) 215–222.
[9] Z. Dong, X. Le, Y. Liu, C. Dong, J. Ma, J. Mater. Chem. A 2 (2014) 18775–18785.
[10] C.B. Molina, A.H. Pizarro, J.A. Casas, J.J. Rodriguez, Appl. Catal. B 148–149 (2014) 330–338.
[11] B. Yang, S. Deng, G. Yu, Y. Lu, H. Zhang, J. Xiao, G. Chen, X. Cheng, L. Shi, Chem. Eng. J. 219 (2013) 492–498.
[12] J.A. Baeza, L. Calvo, J.J. Rodriguez, E. Carbó-Argibay, J. Rivas, M.A. Gilarranz, Appl. Catal. B 168–169 (2015) 283–292.
[13] J.A. Baeza, L. Calvo, J.J. Rodriguez, M.A. Gilarranz, Chem. Eng. J. 294 (2016) 40–48.
[14] M. Munoz, Z.M. de Pedro, J.A. Casas, J.J. Rodriguez, Appl. Catal. A 488 (2014) 78–85.
[15] E. Diaz, A.F. Mohedano, J.A. Casas, J.J. Rodriguez, Appl. Catal. B 181 (2016) 429–435.
[16] J. Zhou, K. Wu, W. Wang, Z. Xu, H. Wan, S. Zheng, Appl. Catal. A 470 (2014) 336–343.
[17] J.A. Baeza, L. Calvo, M.A. Gilarranz, A.F. Mohedano, J.A. Casas, J.J. Rodriguez, J. Catal. 293 (2012) 85–93.
[18] E. Díaz, J.A. Casas, Á.F. Mohedano, L. Calvo, M.A. Gilarranz, J.J. Rodríguez, Ind. Eng. Chem. Res. 47 (2008) 3840–3846.
[19] J.A. Baeza, L. Calvo, M.A. Gilarranz, J.J. Rodriguez, Chem. Eng. J. 240 (2014) 271–280.
[20] A.J. Biacchi, R.E. Schaak, ACS Nano 5 (2011) 8089–8099.
[21] Y. Ren, G. Fan, C. Wang, J. Hazard. Mater. 274 (2014) 32–40.
[22] E. Diaz, A.F. Mohedano, J.A. Casas, L. Calvo, M.A. Gilarranz, J.J. Rodriguez, Appl. Catal. B 106 (2011) 469–475.
[23] G.S. Pozan, I. Boz, J. Hazard. Mater. 136 (2006) 917–921.
[24] E. Díaz, J.A. Casas, Á.F. Mohedano, L. Calvo, M.A. Gilarranz, J.J. Rodríguez, Ind. Eng. Chem. Res. 48 (2009) 3351–3358.
[25] D. Fang, W. Li, J. Zhao, S. Liu, X. Ma, J. Xu, C. Xia, RSC Adv. 4 (2014) 59204–59210.
[26] G. Fan, Y. Ren, W. Jiang, C. Wang, B. Xu, F. Liu, Catal. Commun. 52 (2014) 22–25.
[27] C.B. Molina, A.H. Pizarro, M.A. Gilarranz, J.A. Casas, J.J. Rodriguez, Chem. Eng. J. 160 (2010) 578–585.
[28] H. Deng, G. Fan, C. Wang, L. Zhang, Catal. Commun. 46 (2014) 219–223.
[29] Q. Peng, J. Guo, Q. Zhang, J. Xiang, B. Liu, A. Zhou, R. Liu, Y. Tian, J. Am. Chem. Soc. 136 (2014) 4113–4116.
[30] X. Li, C. Zeng, G. Fan, Int. J. Hydrogen Energy 40 (2015) 9217–9224.
[31] X. Xie, Y. Xue, L. Li, S. Chen, Y. Nie, W. Ding, Z. Wei, Nanoscale 6 (2014) 11035–11040.
[32] M. Naguib, V.N. Mochalin, M.W. Barsoum, Y. Gogotsi, Adv. Mater. 26 (2014) 992–1005.
[33] D. Er, J. Li, M. Naguib, Y. Gogotsi, V.B. Shenoy, ACS Appl. Mat. Interfaces 6 (2014) 11173–11179.
[34] X. Xie, S. Chen, W. Ding, Y. Nie, Z. Wei, Chem. Commun. 49 (2013) 10112–10114.
[35] M. Naguib, O. Mashtalir, J. Carle, V. Presser, J. Lu, L. Hultman, Y. Gogotsi, M.W. Barsoum, ACS Nano 6 (2012) 1322–1331.
[36] G. Zou, Z. Zhang, J. Guo, B. Liu, Q. Zhang, C. Fernandez, Q. Peng, ACS Appl. Mater. Interfaces 8 (2016) 22280–22286.
[37] E. Satheeshkumar, T. Makaryan, A. Melikyan, H. Minassian, Y. Gogotsi, M. Yoshimura, Sci. Rep. 6 (2016) 32049.
[38] H. Sun, L. Cao, L. Lu, Nano Res. 4 (2011) 550–562.
[39] R.B. Rakhi, B. Ahmed, M.N. Hedhili, D.H. Anjum, H.N. Alshareef, Chem. Mater. 27 (2015) 5314–5323.
[40] Y. Liu, W. Wang, Y. Ying, Y. Wang, X. Peng, Dalton Trans. 44 (2015) 7123–7126.
[41] F. Pan, W. Zhang, J. Ma, N. Yao, L. Xu, Y.-S. He, X. Yang, Z.-F. Ma, Electrochim. Acta 196 (2016) 572–578.
[42] Y. Tang, J. Zhu, C. Yang, F. Wang, J. Electrochem. Soc. 163 (2016) A1975–A1982.
[43] P. Giannoccaro, M. Gargano, A. Fanizzi, C. Ferragina, A. Leoci, M. Aresta, J. Mol. Catal. A: Chem. 227 (2005) 133–140.
[44] H.J. Gysling, J.R. Monnier, G. Apai, J. Catal. 103 (1987) 407–418.
[45] X. Xu, X. Li, H. Gu, Z. Huang, X. Yan, Appl. Catal. A 429–430 (2012) 17–23.
[46] J. Zhu, M. Li, M. Lu, J. Zhu, Catal. Sci.Technol. 3 (2013) 737–744.
[47] X. Cui, W. Zuo, M. Tian, Z. Dong, J. Ma, J. Mol. Catal. A: Chem. 423 (2016) 386–392.
[48] G. Yuan, M.A. Keane, Catal. Commun. 4 (2003) 195–201.
[49] H.-L. Lien, W.-X. Zhang, Appl. Catal. B 77 (2007) 110–116.
[50] M.A. Keane, G. Pina, G. Tavoularis, Appl. Catal. B 48 (2004) 275–286.
[51] S. Ordóñez, E. Díaz, R.F. Bueres, E. Asedegbega-Nieto, H. Sastre, J. Catal. 272 (2017) 158–168.
[52] E. Diaz, A.F. Mohedano, J.A. Casas, C. Shalaby, S. Eser, J.J. Rodriguez, Appl. Catal. B 186 (2016) 151–156.